Fabrication and Performance of an FBG-based Effective Stress Cell for Directly Measuring Effective Stress in Saturated Soils

by

Jie-Qiong QIN[1] (Ph.D.)

[1]Department of Civil and Environmental Engineering

The Hong Kong Polytechnic University, Hung Hom, Kowloon, Hong Kong, China

Email: jieqiong.qin@connect.polyu.hk

Wei-Qiang FENG[1] (Post-Doctoral Fellow and Corresponding Author)

[1]Department of Civil and Environmental Engineering,

The Hong Kong Polytechnic University, Hung Hom, Kowloon, Hong Kong. China

Email: wqfeng@polyu.edu.hk

Pei-Chen WU (Ph.D. Candidate)

Department of Civil and Environmental Engineering

The Hong Kong Polytechnic University, Hung Hom, Kowloon, Hong Kong, China

Email: 16900045r@connect.polyu.hk

and

Jian-Hua YIN[1] (Chair Professor)

[1]Department of Civil and Environmental Engineering

The Hong Kong Polytechnic University, Hung Hom, Kowloon, Hong Kong, China

Tel: (852) 2766-6065, Fax: (852) 2334-6389, Email: cejhyin@polyu.edu.hk

ABSTRACT

Effective stress is a crucial parameter in safety and stability assessments of geotechnical structures. In this paper, a novel stress cell based on fiber Bragg grating (FBG) sensing technology is manufactured and calibrated for the direct measurement of effective stress in saturated soils. The novel effective stress cell (ESC) mainly includes the stainless-steel sensing plate, porous disc, and FBG sensor. Because of the counteraction of pore-water pressures acting on the outer and inner surfaces of sensing plate, the thin plate theory can be utilized to determine the effective stress of soil skeleton directly. The feasibility of FBG-ESC was verified by conducting one physical model test. The measured data from the FBG-ESC agree well with the calculation results from the measured total earth pressure and excess pore-water pressure provided by the conventional transducers. Furthermore, the FBG-ESC was applied in one physical model to monitor the evolution of effective stress of clayey soils subjected to complicated loadings.

Keywords: effective stress, fiber Bragg grating, clayey soil, effective stress cell

1 Introduction

Settlement and stability of geotechnical structures, for instance, foundations, tunnels, and slopes are of great concern for geotechnical engineers. They are closely associated with stress-strain state, volume change, and strength behavior of soils which are directly related to the effective stresses in soils [1]. The effective stresses are the average stresses undertaken by the soil skeleton, independent of the excess pore-water pressure. Hence, a good understanding and evaluation of the effective stress play a vital role in safety and stability assessments of the geotechnical structures. However, the effective stresses in soils are normally determined by subtracting the measured pore-water pressure from the measured total earth pressure. So far, there is no geotechnical instrument for directly measuring the effective stresses.

Over the past decades, a variety of electrical instruments based on vibrating wire or electrical strain gauges have been developed and widely employed for total earth pressure and pore-water pressure measurements, mainly in soil pressure cells [2–4], piezometers and miniature pore-water pressure transducers. Nevertheless, the existing electrical sensors are being replaced by fiber optic sensors owing to their inherent drawbacks of sensitivity to electromagnetic interference, low reliability for long term sensing, signal loss in long distance transmission, and a large quantity of electrical cables for multi-point measurements [5].

In recent years, fiber optic sensing technology, especially fiber Bragg grating (FBG) sensing technology, is undergoing a rapid development in geotechnical engineering. Compared with the electrical sensors, fiber optic sensors are more suitable for the harsh geotechnical environment due to their superiority in accuracy, reliability, capability of multiplexing and

immunity to electromagnetic interference [5–7]. Several pressure sensors based on fiber optic sensing technology have been developed to measure total earth pressure [8,9] and pore-water pressure [10]. Recently, Correia et al. [11] reported an FBG-based soil pressure sensor by using two diaphragms as the sensing elements for independent measurement of the total earth pressure and pore-water pressure. It should be noted that the effective stress is still calculated by subtracting the pore-water pressure from the total earth pressure. Therefore, this method is still an indirect measurement.

In this study, a diaphragm-type pressure cell based on FBG sensing technology is fabricated, calibrated, and implemented for direct measurement of effective stress in saturated soils. The FBG sensor is attached at the center of a sensing plate and utilized to detect the strains with the applied pressures. The working principle of the FBG-based effective stress cell (ESC), test setup, and results are described in detail and discussed. To investigate the work feasibility and performance of the proposed FBG-ESC, a physical model test is conducted on a saturated Completely Decomposed Granite (CDG) soil with the installation of a conventional earth pressure transducer (EPT) and pore-water pressure transducers (PPTs). Finally, the FBG-ESC is applied in the Hong Kong Marine Deposits (HKMD) improved by prefabricated vertical drains (PVDs) in a physical model with plane strain condition to monitor the evolution of effective stress.

2 Working principle of FBG sensor and FBG-based effective stress cell

2.1 Working principle of FBG sensor

Bragg grating is written into the core of an optical fiber by exposing the core to an intense optical interference pattern, such as a spatial pattern of ultraviolet (UV) light. The formed permanent grating incurs a periodic perturbation of the core refractive index along the fiber length [12]. According to Bragg's law, when the fiber with an FBG sensor is illuminated by a spectrally broadband source of light, a narrow spectral component at the Bragg wavelength is reflected by the grating which acts as a narrowband reflection filter. As a result, this narrow spectral component disappears in the transmitted light [13], as depicted in Figure 1. The rationale of operating an FBG-based sensor system is to detect the wavelength shift of reflected "Bragg" light as a function of the measurand. The Bragg wavelength is determined by the expression

$$\lambda_B = 2\mathrm{n}_{eff}\Lambda \tag{1}$$

where λ_B is the Bragg wavelength, typically in a range of 1510 nm - 1590 nm; n_{eff} is the effective refraction index; and Λ is the grating pitch.

The shift in Bragg wavelength is related to strain and temperature changes. Strain causes the changes in grating pitch and fiber index due to the physical elongation of the sensor and photo-elastic effects, while temperature incurs the thermal expansion of the fiber material and the shift in refractive index which is temperature-related [14]. For a single mode silica fiber, the relationship between the shift in Bragg wavelength and the changes of strain and temperature exhibits linearity and is expressed as Othonos [15]:

$$\frac{\Delta\lambda_B}{\lambda_{B0}} = C_\varepsilon \Delta\varepsilon + C_T \Delta T \tag{2}$$

where λ_{B0} is the Bragg wavelength at the initial state; $\Delta\lambda_B$ is the wavelength shift induced by the strain change $\Delta\varepsilon$ and temperature variation ΔT; C_ε and C_T are the coefficients corresponding to strain and temperature with the typical values of 0.78 and $6.67\times10^{-6}/°C$, respectively.

2.2 Working principle of FBG-based effective stress cell

In the design, the ESC consists of a sensing plate with the FBG sensor, a perforated disc base, and a rigid ring, as illustrated in Figure 2. The thin plate acts as a sensing element where the FBG sensor is adhered, while the porous disc base works as a filter to insulate soil particles from the inside of the cell. Owing to the porous disc base, only pore-water pressure is acted on the inner surface of the sensing plate while total earth pressure, which is the sum of pore-water pressure and effective stress in soils, is applied on the outer surface of the plate in the opposite direction. The pore-water pressures acted on the two surfaces of sensing plate have the same absolute value but with opposite signs, thus balance of pressures on the two surfaces is equal to effective stress and the strain measured by FBG sensor is only induced by the effective stress.

Figure 3 shows working principle of effective stress cell in saturated soils. Assumed that the pressure is uniformly exerted over the dimensions of the sensing plate, the thin plate theory can be utilized [16]. The deflection (ω) of the circular thin plate with clamped edges is calculated as

$$\omega = \frac{\sigma}{64D}\left(a^2 - r^2\right)^2. \tag{3}$$

where σ denotes the uniform stress, D is bending stiffness of the plate: $D = Eh^3/12\left(1-\upsilon^2\right)$, E and υ are elastic modulus and Poisson's ratio of the plate material, respectively; h is the thickness of the circular plate and a is the radius of the plate and r is the distance from the center of the plate. Referring to compatibility of geometry, the strain in radial direction is $\varepsilon_r = z\,d\theta/dr$, where z is the distance from the neutral axis. For the small deflection, the slope of the deformed plate is given by $-d\omega/dr = \tan\theta = \theta$. Therefore, the radial strain is deduced as

$$\varepsilon_r = -z\frac{d^2\omega}{dr^2} = \frac{\sigma z}{16D}\left(a^2 - 3r^2\right) \tag{4}$$

Considering the FBG sensor was adhered at the center of the plate, the strain is obtained by

$$\varepsilon_{r,\max} = \varepsilon_{r,r=0} = z\frac{\sigma}{16D}a^2 = \frac{h}{2}\frac{\sigma}{16D}a^2 = \frac{\sigma}{32D}ha^2 \tag{5}$$

where $z = h/2$. Substituting $\Delta\varepsilon = \left(\Delta P \cdot ha^2\right)/32D$ into Eq. (2), the relationship of the shift in Bragg wavelength and applied pressure is given as

$$\Delta\lambda_B = C_\varepsilon\frac{\Delta\sigma}{32D}\lambda_{B0}ha^2 + C_T\Delta T\lambda_{B0} \tag{6}$$

Eq. (6) can be written as

$$\sigma' = \frac{32D}{C_\varepsilon ha^2\lambda_{B0}}\left(\Delta\lambda_B - C_T\Delta T\lambda_{B0}\right) \tag{7}$$

It is noted that the FBG-ESC was fabricated, calibrated, and applied in the laboratory with a constant temperature of 20 °C. The separation of the temperature from strain is done by placing an FBG into a metallic tube so that the FBG has no contact with the structure with straining. In this way, the temperature is measured and used to compensate temperature effect. After the

139 temperature compensation. It is indicated that λ_{B0} is constant for a specified FBG sensor.
140 Hence, the shift in Bragg wavelength is proportion to the applied pressure. Since the deflection
141 of sensing plate is only induced because of the counteraction of pore-water pressures, this novel
142 cell can be used for direct measurement of effective stress in soils.

143

144

145 4 Calibration of FBG-based effective stress cell

146 In this study, the ESC is fabricated with the external diameter of 120 mm and thickness of 16
147 mm. The thin plate in disc groove is 100 mm in diameter and 1 mm in thickness and the porous
148 disc base is 120 mm in diameter and 2 mm in thickness. All parts were made of 316 stainless-
149 steel material with elastic modulus of 193 GPa and Poisson's ratio of 0.3. The yield strain of
150 316 stainless-steel is ± 1050 με. With the Eq. (7), the allowable pressure range of the FBG-
151 ESC is 201.9 kPa. A 10 mm long FBG sensor with a central wavelength range of 1542 nm was
152 attached to the center of inner surface of the thin plate and protected well by epoxy adhesives.
153 In consideration of multiplexing, the FBG sensor was connected with a two-core single mode
154 fiber by using an arc fusion splicer. (Figure 4 does not mention in the manuscript)

155 The effective stress cell described herein can provide the advantages as: (1) novel design. (分
156 号可以用在逗号的后面吗？) This FBG-based effective stress cell is capable of direct
157 measurement of effective stress in soils by using one diaphragm only; (2) multiplexing capacity.
158 Because the FBG sensors can be connected in series and can measure the strain or temperature

159 at multi-points along one fiber line; (3) Direct measurement of effective stress at one location
160 rather two locations using most other conventional transducers; (3) high accuracy due to the
161 high resolution of FBG sensors (e.g., 1×10-6 strain); (4) high reliability and durability due to
162 the long-term stability of FBG sensors. The application of fiber Bragg grating (FBG) sensing
163 technology has advantages, e.g., the immunity to electromagnetic interference, long-term
164 stability, high accuracy and small size etc., which benefit the accuracy and feasibility of the
165 novel FBG-based effective stress cell.

166 **4.1 Setup of calibration test**

167 In previous researches, calibration tests of soil pressure transducers were mostly conducted by
168 employing gas [17, 11], water [18], oil [8] or sand [9] as the loading medium. In this study, the
169 FBG-ESC was calibrated by applying water pressure. Figure 5(a) presents the test apparatus
170 for the calibration, including a water container, a Geotechnical digital system (GDS) pressure
171 controller (GDS Instruments Ltd.), and an optical sensing interrogator (Micro Optics Inc.,
172 SM125). Calibration tests were conducted in the 300 mm in diameter and 500 mm in height
173 water container whose cover has a tube. The tube was connected with the GDS pressure
174 controller which can provide a stable water pressure with a resolution of 1 kPa and a pressure
175 range of 2000 kPa. G-clamps and an O-ring were used to ensure a good sealing performance
176 of the container. The optical fiber was connected to the optical sensing interrogator which
177 provides a broadband source of light and detects the reflected signal simultaneously at a
178 frequency of 1 Hz. The FBG-ESC was placed in the water container at the depth of 250 mm,
179 as illustrated in Figure 5(b).

It is crucial to control the difference of water pressures acting on the inner and outer surface of sensing plate. A solid disc base was employed to replace the porous disc base in the calibration tests. The groove and the solid disc base were fitted together and sealed well by an O-ring. Although there was air trapped in the sealed cell and slightly pressured by movement of the sensing plate during tests, the influence of the pressured air was negligible due to small amounts of trapped air and high stiffness of the sensing plate. The water pressures from 0 to 200 kPa at 20 kPa increments were applied in the calibration. In order to evaluate the repeatability of the FBG-ESC and obtain an exact value of coefficient, two cycles including loading and unloading were conducted.

4.2 Results of calibration test

Figure 6 shows the calibration results plotted for both loading and unloading. The results of two loading-unloading cycles exhibit that the designed FBG-ESC has a good repeatability. It is found that there is a linear relationship between the reflected Bragg wavelength and applied water pressure, which demonstrates the agreement with the Eq. (9). The reflected Bragg wavelength rises from 1541.94 nm to 1542.58 nm with the increased water pressure from 0 kPa to 200 kPa. Using the least-squares method, a linear transfer function with a good coefficient of determination (COD should we use R^2?) value of 0.9954 is obtained and shown in Figure 6. From the transfer function, the pressure sensitivity of the FBG-based effective stress cell is 3.2 pm/kPa, and the pressure resolution of this effective stress cell is 0.31 kPa when the FBG sensor is interrogated by the optical sensing interrogator (SM125) which has a 1 pm wavelength resolution. According to Eq. (7), the theoretical pressure sensitivity is 5.3

pm/kPa. There is a small discrepancy between the pressure sensitivities in theoretical analysis and calibration tests. The reasons mainly include that: (a) the strain measured by the FBG sensor is average strain within the length of 10 mm; and (b) the adhesive strength and thickness of epoxy adhesives affect the response of FBG sensor to the applied water pressure.

5 Verification of the novel effective stress cell in a physical model test

5.1 Physical model setup

A physical model test was carried out to verify the workability and accuracy of the FBG-ESC in geotechnical environment. As shown in Figure 7, the cylindrical physical model is made of stainless steel and has the diameter of 300 mm and the height of 450 mm. Lubricating oil and a flexible plastic film were also applied over the inner surface of the cylindrical physical model to reduce the friction between the soil and the inner surface. A fully saturated Completely Decomposed Granite (CDG) soil was used in the physical model test. The basic properties of the CDG soil are listed in Table 1. Calibration tests of all the conventional transducers used in the physical model test were conducted by applying water pressure. The earth pressure transducers (EPT1 and EPT2) and the mini pore-water pressure transducer (PPT3) were calibrated in a sealed Perspex cylinder with water pressure provided by a GDS pressure/volume controller (model STDDPC), while the pore-water pressure transducers (PPT1 and PPT2) were calibrated by applying water pressure through directly connecting with the GDS pressure/volume controller. A pressure calibrator (model Fluke 718 300G, Fluke Calibration) was utilized to calibrate all the conventional transducers. The calibrated results are shown in Figure 8.

222 The new FBG-ESC was placed in fully saturated CDG soil at the height of 250 mm, in company
223 with a conventional mini earth pressure transducer (EPT2) and a conventional mini pore-water
224 pressure transducer (PPT3). A reaction frame loading system, including a pneumatic jack, was
225 set up on the cylindrical physical model, as shown in Fig. 7. An air pressure regulator was
226 employed to control the air pressure inside the pneumatic jack and a load cell was installed to
227 monitor the applied vertical loads provided by the pneumatic jack. In order to ensure the
228 uniformity of the applied overburden pressure and soil deformation as well as water drainage,
229 a layer of sand and a perforated stainless-steel plate were placed on the top of the saturated
230 CDG soil. During testing, the same optical sensing interrogator (SM125) and data logger (NI
231 PXIe-4331) were used for data acquisition. In preparation stage, an average overburden
232 pressure of 5 kPa was exerted on the top of the saturated CDG soil by using dead weights to
233 establish the contact of all transducers with surrounding soils. Afterwards, a multi-stage
234 overburden pressure was imposed in the following process. The first stage with an average
235 overburden pressure of 60 kPa was carried out and lasted for 190 hours. In the second stage,
236 the overburden pressure rose from 60 kPa to 120 kPa and was kept at 120 kPa for 160 hours.
237 Afterwards, the complicated overburden pressure is controlled by the air pressure regulator to
238 examine the performance of ESC in saturated soils subjected a complicated loading condition.

239 **5.2 Results and discussion**

240 Figure 9 displays the test results under the multi-stage average overburden pressure. It is seen
241 that the total stress measured by the conventional earth pressure cell (EPT2) is identical to the
242 applied pressure. In both stages, the excess pore-water pressure was gradually dissipated and

243 decreased to 0 kPa, and the effective stress was accordingly increasing. By comparison, the
244 directly measured effective stress by the FBG effective stress cell fairly agrees with the
245 calculated effective stress obtained based on the measured total stress and pore-water pressure,
246 as illustrated in Fig 9b. It is observed that during the initial loading period of each stage, the
247 effective stress measured by the FBG effective stress cell has a difference to the calculated
248 effective stress. The small discrepancy primarily arises from the reliability of the calculated
249 results which are based on measured total stress and porewater pressure. Errors may occur in
250 the results since the response time of the conventional transducers (EPT2 and PPT3) to the
251 applied pressure is not identical. Therefore, the newly developed FBG-ESC, as a direct
252 measurement method, has a better performance compared with the calculated effective stress
253 by using the indirect measurement method.

254 Figure 10 plots the measured results of conventional transducers and FBG-ESC in the physical
255 model of CDG soils under the complex overburden pressures. Similar performance in Figure
256 9 is found in the physical model test under the complex loading condition. Different durations
257 of loading and unloading from 65 kPa to 20 kPa were examined by using the conventional and
258 newly designed transducers. The good agreement of measured data from FBG-ESC and
259 calculated values of effective stress demonstrates that the new FBG-ESC can be utilized in
260 saturated soils subjected to complex loading conditions. Furthermore, the effective stress can
261 be directly obtained with less disturbance on a soil by making use of a single FBG-ESC, in
262 comparison with embedding two cells of both an earth pressure transducer and a pore-water
263 pressure transducer. The uncertainties from two different measurement locations of both an
264 earth pressure transducer and a pore-water pressure transducer can be effectively eliminated as

well. Therefore, this newly developed FBG-ESC which can measure the effective stress in a single cell and be placed at one location can provide better and more reliable measurement of the effective stress in saturated soils.

6 Application of the novel effective stress cell

6.1 Physical model and procedures

A physical model test was carried out to verify the workability and accuracy of the FBG-ESC in geotechnical environment. In this study, a rectangular box consisting of two steel walls, two transparent plastic walls and a steel bottom plate was used for the physical model [10]. The plastic walls are restrained by two steel trusses clamping at the quarter points to prevent swelling and distortion. The dimension of the rectangular box is 900 mm × 300 mm × 870 mm, and an alluvium plate with uniform holes are placed on top of it. Lubricating oil was also spread on the stainless-steel sheet and transparent plastic walls to reduce the friction between the soil and the sides of the container. A fully saturated Hong Kong Marine Deposits (HKMD), taken from East Coast of Lantau Island, was utilized in the physical model tests. The basic properties of the HKMD are listed in Table 2. (table 2 is missing)

The physical model is designed to simulate a double-layered clay improved by prefabricate vertical drains (PVDs) in a square pattern under complicated loading process. A uniformly sand fill layer was placed between the soft soil layer and the alluvium plate. To prevent the interface mix of sand and clay, a layer of geotextile was installed as a separation between the sand layer and clay [19]. Drainage is only allowed from the top surface. The surcharge loading is

applied by dead weights on the top of the alluvium plate in the model. Firstly, the 10 kPa loading was applied and maintained for 50 days, subsequently, the dead loading of 10 kPa was unloaded for 26 days, lastly, the surcharge loading was reloaded to 20 kPa to keep 84 days. The self-weight of HKMD, sand layer and alluvium plate would produce 4.5 kPa

The new FBG-ESC and conventional transducers were calibrated as repeated in Section 5. The arrangement of the transducers is presented in Figure 12(a), which is placed in the bottom of the physical model. In the physical model test, the FBG-ESC was interrogated by the optical sensing interrogator (SM130), and the data of conventional transducers were acquired by the data logger (NI PXIe-4331, supplied by National Instruments Co.), as illustrated in Figure 12(b).

6.2 Results and Interpretation

Figure 13 presents the measured data of conventional transducers and compares the calculated results with measured data of FBG -ESC in HKMD subjected to a complex loading process including loading, unloading and reloading. The applied loading is plotted based on the dead load and self-weight of HKMD, sand layer and alluvium plate. The pore-water pressure gradually dissipates with time, as shown in Figure 13(a). Because the permeability of HKMD is much lower than that of CDG, the consolidation duration of this physical model is obvious larger than the time in cylinder physical model with saturated CDG soil.

Because the HKMD is saturated, effective stress can be calculated by subtracting the pore-water pressure from the total applied loading. In comparison, the effective stress was also

directly monitored during the loading process in the test. The values of effective stress increase gradually with time, showing that the applied pressure is transferred to the soil skeleton during the process of excess pore-water pressure dissipation. The data from FBG-ESC generally agree well with the calculation results based on applied loading and excess pore water pressure. The gap is less than 4 kPa, which may be mainly due to side friction in the physical model. Moreover, the performance of FBG-ESC in the unloading stage is also examined in Figure 13(b). It is observed that the data of FBG-ESC is more stable than that of calculated results. Importantly, the FBG-ESC could provide the valuable data in the physical model to analysis the settlement of saturated soils.

7 Conclusions

In this study, the design principle and calibration of the FBG- based effective stress cell (FBG-ESC) for direct measurement of effective stress in soil have been presented. The primary concept of this design is the counteraction of pore-water pressures acting on the outer and inner surfaces of sensing plate. The calibration of the FBG-based effective stress cell was conducted by employing water pressure. The working performance of the FBG-ESC is elaborated in a cylinder physical model with a saturated Completely Decomposed Granite (CDG). Moreover, theother physical model test was conducted to examine the workability and performance of the proposed FBG-ESC in a clayey soil.

Acknowledgement

The work in this paper is supported by a CRF project (Grant No.: PolyU 12/CRF/13E) from Research Grants Council (RGC) of Hong Kong Special Administrative Region Government (HKSARG) of China, two GRF projects (PolyU 152196/14E; PolyU 152796/16E) from RGC of HKSARG of China. The authors also acknowledge the financial supports from Research Institute for Sustainable Urban Development of The Hong Kong Polytechnic University, grants (1-ZVCR, 1-ZVEH, 4-BCAU, 4-BCAW, 5-ZDAF, G-YN97) from The Hong Kong Polytechnic University.

References

[1] Lade, P. V., & De Boer, R. (1997). The concept of effective stress for soil, concrete and rock. *Geotechnique*, *47*(1), 61-78.

[2] Clayton, C. R. I., & Bica, A. V. D. (1993). The design of diaphragm-type boundary total stress cells. *Geotechnique*, *43*(4), 523-535.

[3] Talesnick, M. (2005). Measuring soil contact pressure on a solid boundary and quantifying soil arching. *Geotechnical Testing Journal*, *28*(2), 171-179.

[4] Zhu, B., Jardine, R. J., & Foray, P. (2009). The use of miniature soil stress measuring cells in laboratory applications involving stress reversals. *Soils and Foundations*, *49*(5), 675-688.

[5] Pei, H. F., Teng, J., Yin, J. H., & Chen, R. (2014). A review of previous studies on the applications of optical fiber sensors in geotechnical health monitoring. *Measurement*, *58*, 207-214.

[6] Grattan, K. T. V., & Sun, T. (2000). Fiber optic sensor technology: an overview. *Sensors and Actuators A: Physical*, *82*(1-3), 40-61.

[7] Yin, J. H., Zhu, H. H., Jin, W., Yeung, A., & Mak, L. M. (2007). Performance evaluation of electrical strain gauges and optical fiber sensors in field soil nail pullout tests. In *The HKIE Geotechnical Division Annual Seminar*, 249-254.

[8] Zhou, Z., Wang, H., & Ou, J. (2006). A new kind of FBG-based soil-pressure sensor. In *Optical Fiber Sensors*, ThE90.

[9] Li, F., Du, Y., Zhang, W., & Li, F. (2013). Fiber Bragg grating soil-pressure sensor based on dual L-shaped levers. *Optical Engineering*, *52*(1), 014403.

354 [10] Feng, W. Q., Liu, Z. Y., Tam, H. Y., & Yin, J. H. (2016). The pore water pressure sensor
355 based on Sagnac interferometer with polarization-maintaining photonic crystal fiber for
356 the geotechnical engineering. *Measurement*, *90*, 208-214.
357 [11] Correia, R., Li, J., Staines, S., Chehura, E., James, S. W., Kutner, J., Dewhurst, P., Ferreira,
358 P., & Tatam, R. P. (2009). Fibre Bragg grating based effective soil pressure sensor for
359 geotechnical applications. In *20th International Conference on Optical Fibre Sensors*,
360 *7503*, 75030F.
361 [12] Hill, K. O., & Meltz, G. (1997). Fiber Bragg grating technology fundamentals and
362 overview. *Journal of lightwave technology*, *15*(8), 1263-1276.
363 [13] Morey, W. W., Meltz, G., & Glenn, W. H. (1990). Fiber optic Bragg grating sensors.
364 In *Fiber Optic and Laser Sensors VII*, *1169*, 98-108.
365 [14] Kersey, A. D., Davis, M. A., Patrick, H. J., LeBlanc, M., Koo, K. P., Askins, C. G., Putnam,
366 M.A., & Friebele, E. J. (1997). Fiber grating sensors. *Journal of lightwave*
367 *technology*, *15*(8), 1442-1463.
368 [15] Othonos, A. (1997). Fiber bragg gratings. *Review of scientific instruments*, *68*(12), 4309-
369 4341.
370 [16] Timoshenko, S. P., & Woinowsky-Krieger, S. (1959). *Theory of plates and shells*.
371 McGraw-hill.
372 [17] Chang, C. C., Johnson, G., Vohra, S. T., & Althouse, B. (2000). Development of fiber
373 Bragg-grating-based soil pressure transducer for measuring pavement response. In *Smart*
374 *Structures and Materials 2000: Sensory Phenomena and Measurement Instrumentation*
375 *for Smart Structures and Materials*, *3986*, 480-489.

376 [18] Dave, T. N., & Dasaka, S. M. (2013). In-house calibration of pressure transducers and
377 effect of material thickness. *Geomech. Eng*, *5*(1), 1-15.
378 [19] Feng, W. Q., Li, C., Yin, J. H., Chen, J., & Liu, K. (2019). Physical model study on the
379 clay–sand interface without and with geotextile separator. Acta Geotechnica, 1-17.
380

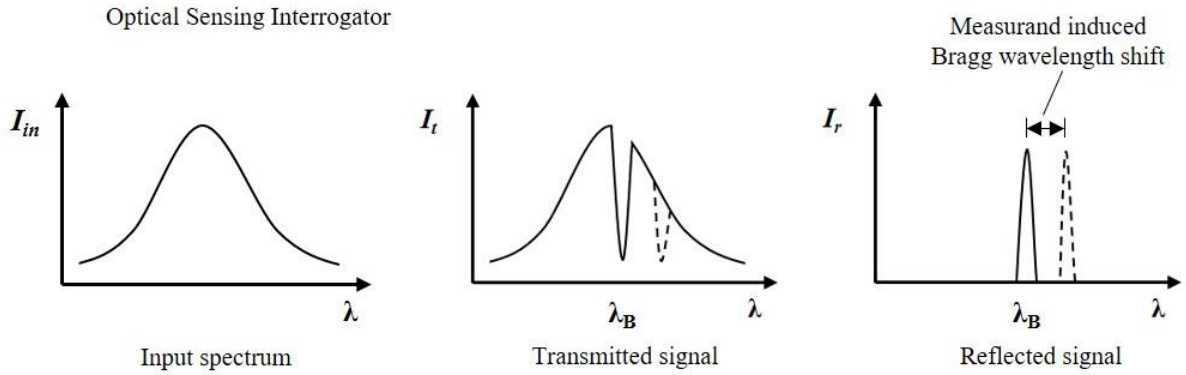

381

382 Figure 1. Schematic illustration of working principle of an FBG sensor
383

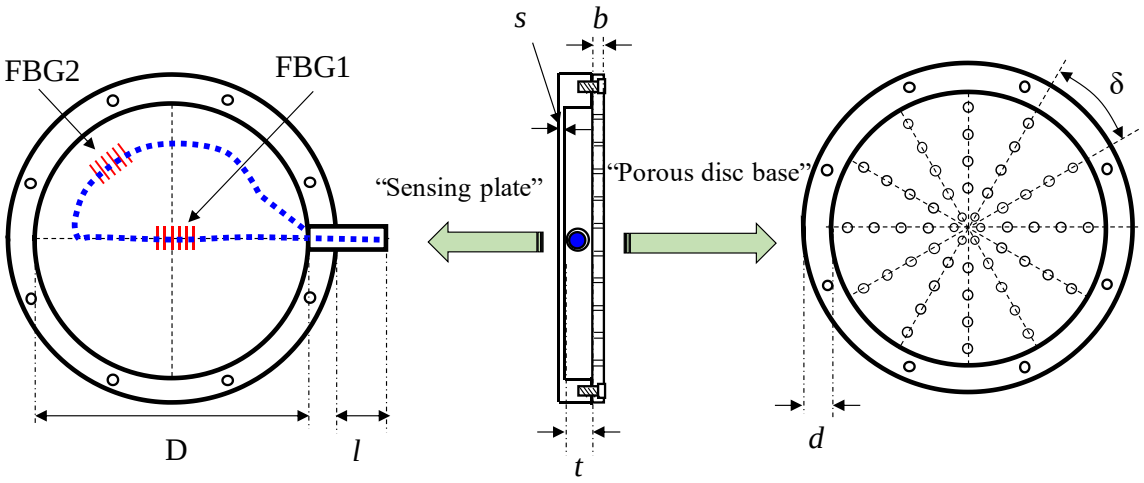

384

385 **Figure 2.** Schematic of an effective stress cell

386

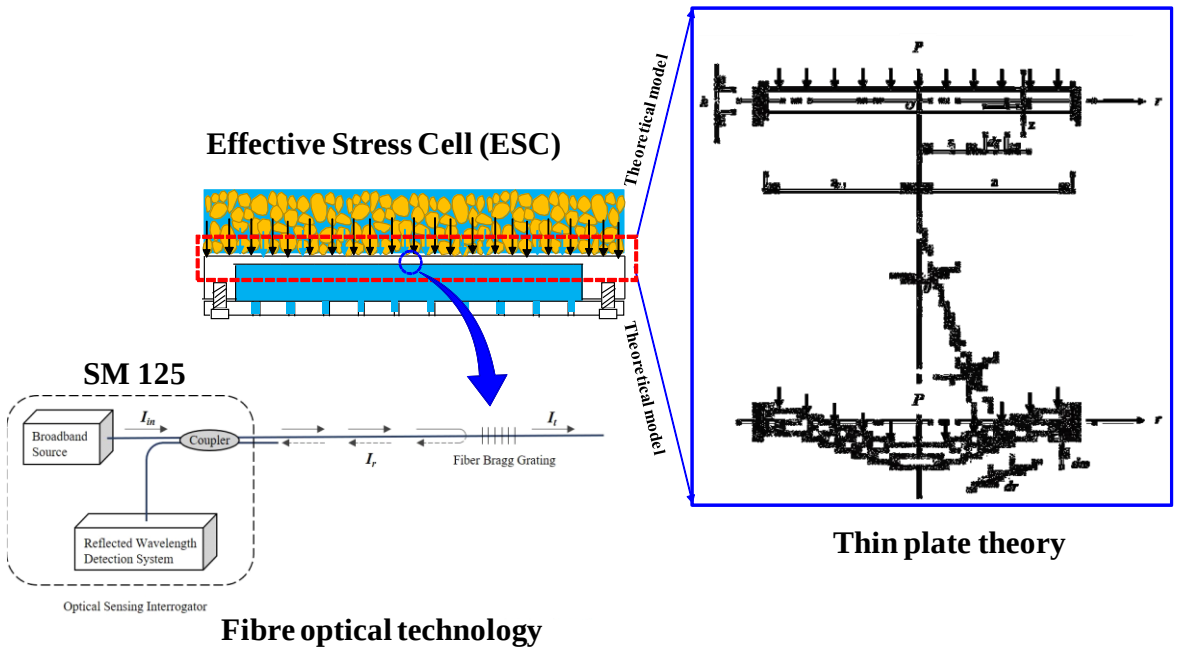

387

388 **Figure 3.** The working principle of effective stress cell subjected to uniform pressure

389

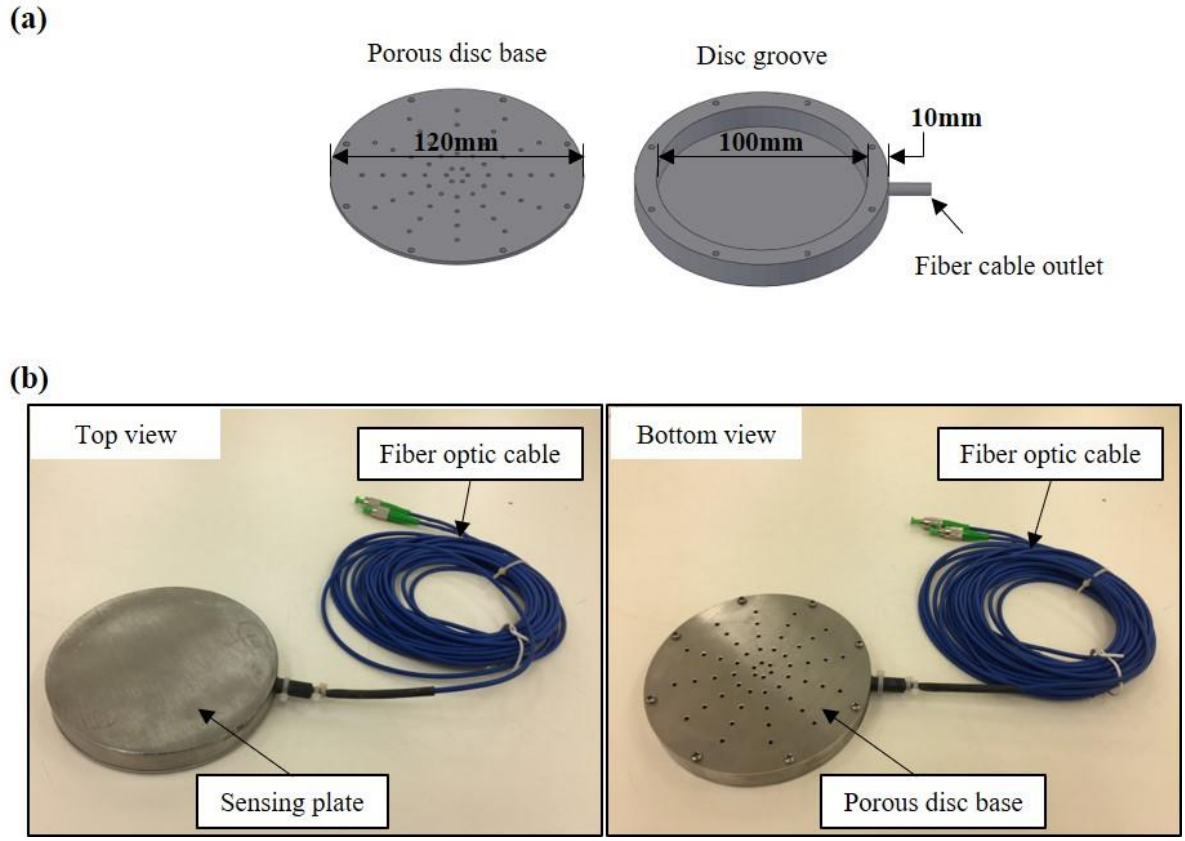

390

391 **Figure 4.** Design of the FBG-based effective stress cell: (a) schematic diagram and (b)
392 photographs
393

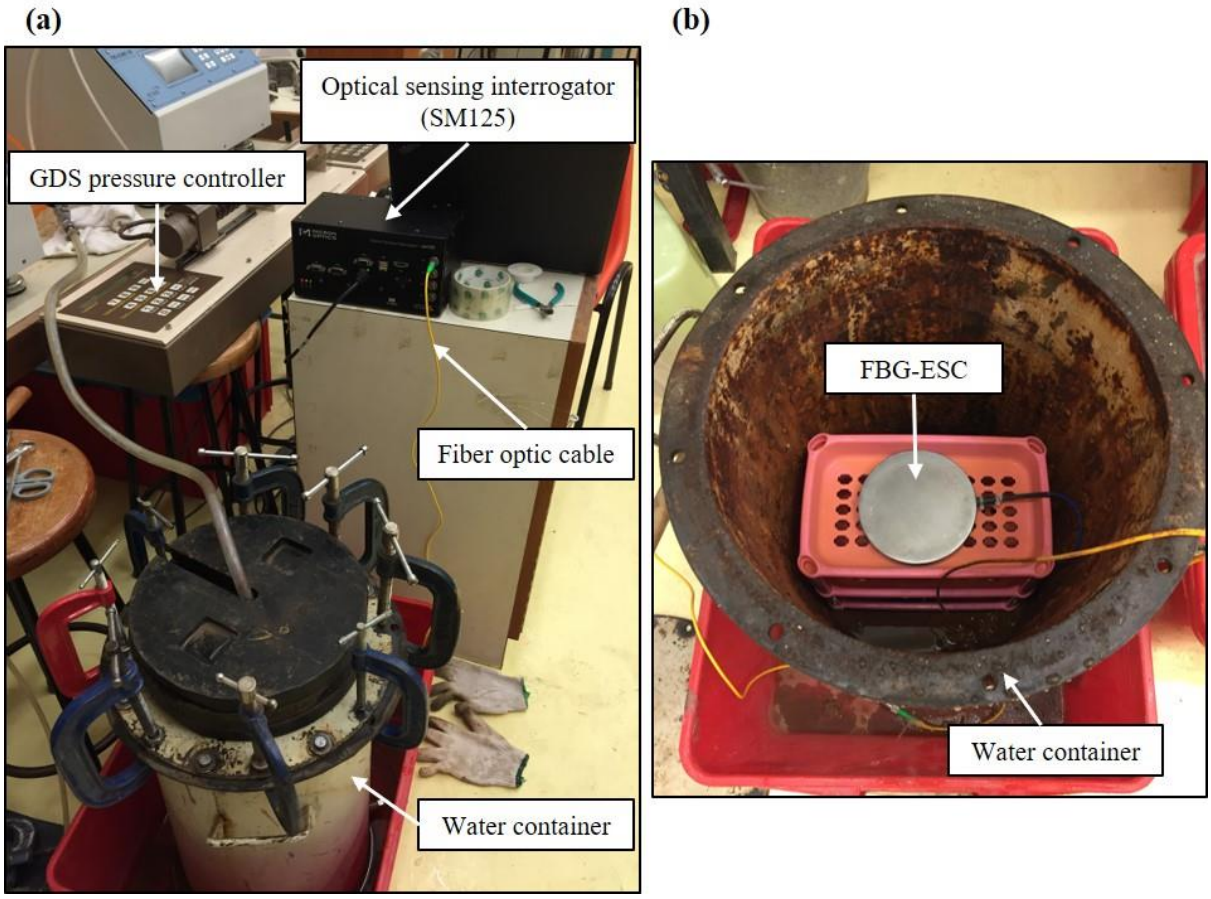

394

395 **Figure 5.** Calibration test setup: (a) test apparatus and (b) the arrangement of the FBG-based
396 effective stress cell (FBG-ESC) in the water container.
397

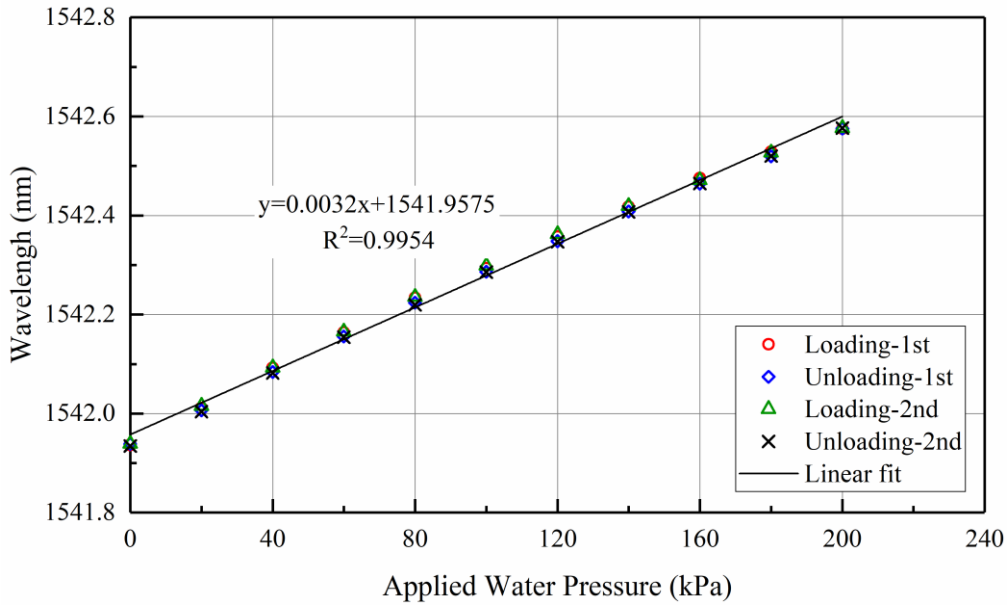

398

399 **Figure 6.** Results of the FBG-based effective stress cell calibration tests

400

401

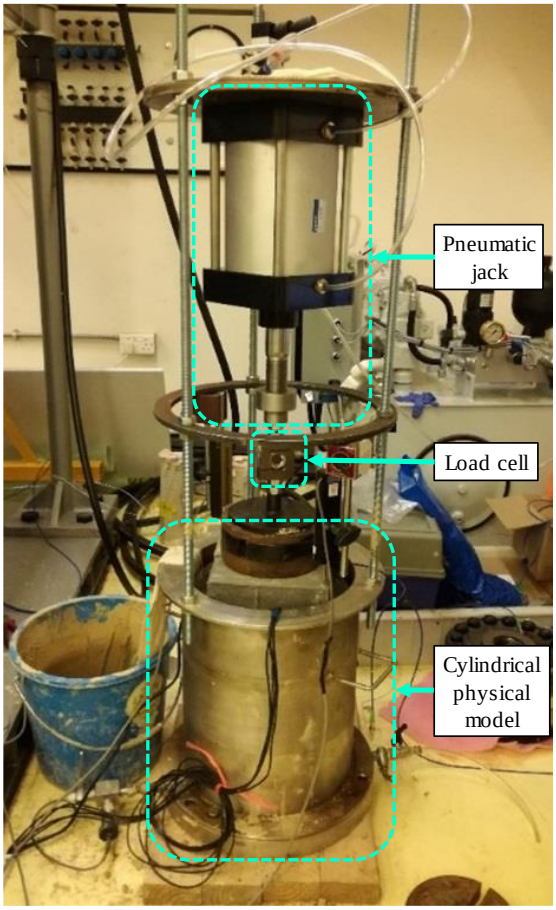

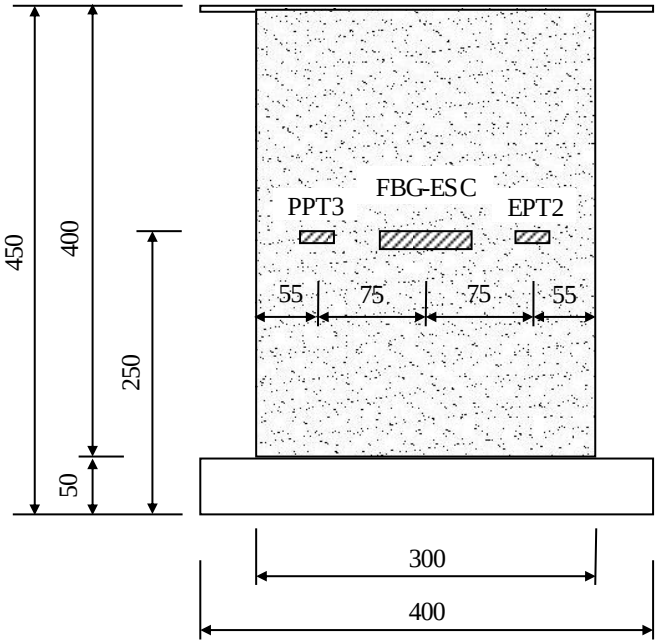

402

403 **Figure 7.** (a)The cylindrical physical model test setup, and (b) the arrangement of the FBG-
404 ESC and the conventional transducers in the cylindrical physical model test
405

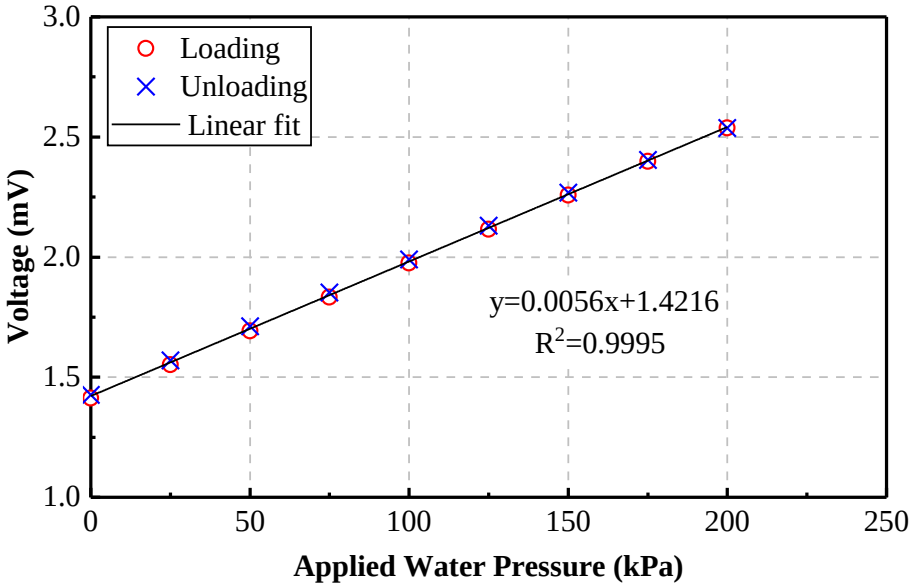

406

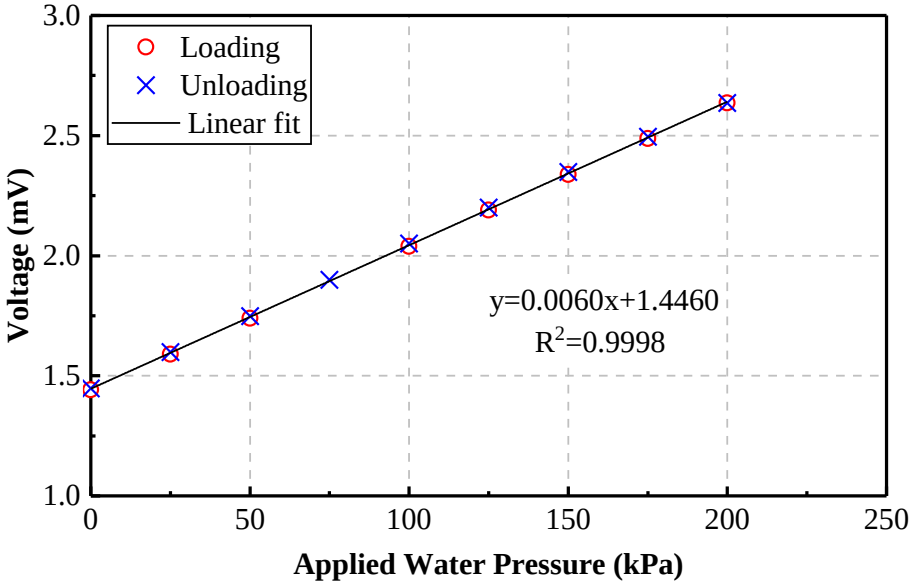

407

408 **Figure 8.** Calibration tests results of the conventional transducers: (a) EPT2, (b) PPT3

409

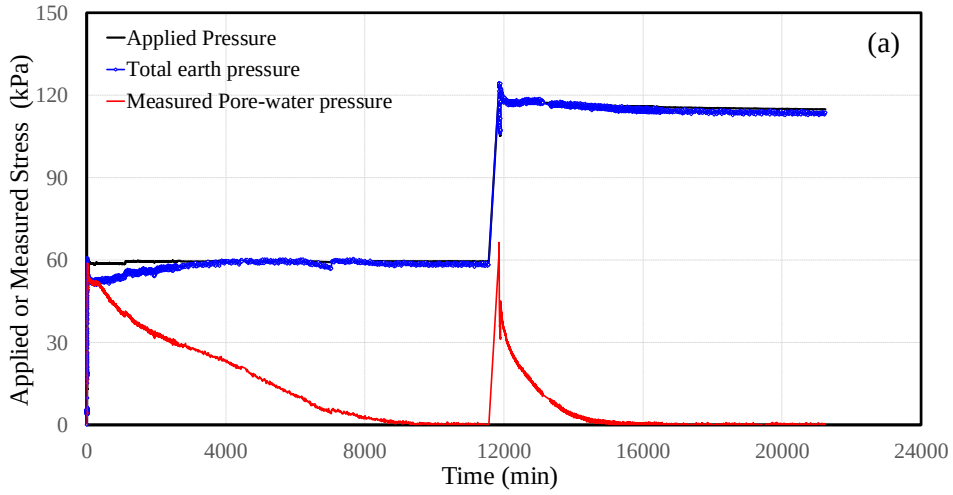

410

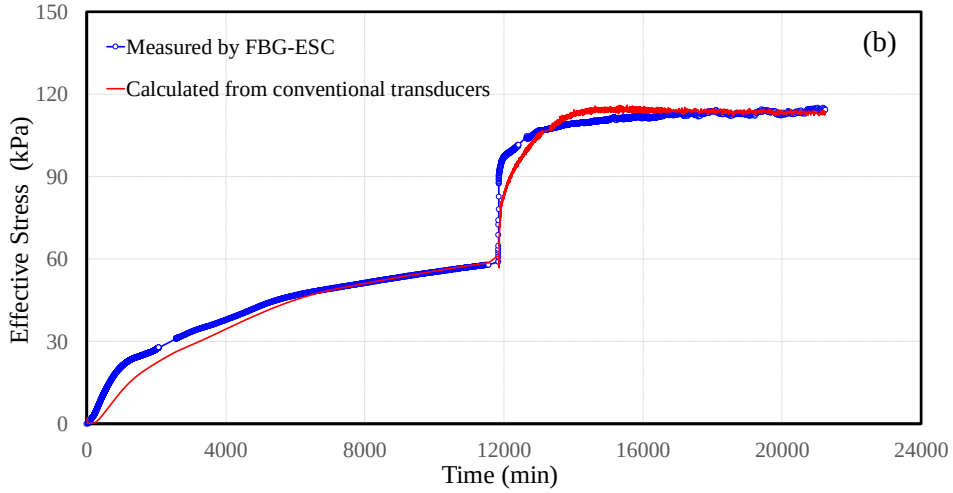

411

412 Figure 9. Test results of the multi-stage overburden pressure in the cylindrical physical model:
413 (a) applied pressure, total stress, and pore-water pressure measured by the conventional
414 transducers and (b) comparison of calculated effective stress and directly measured effective
415 stress

416

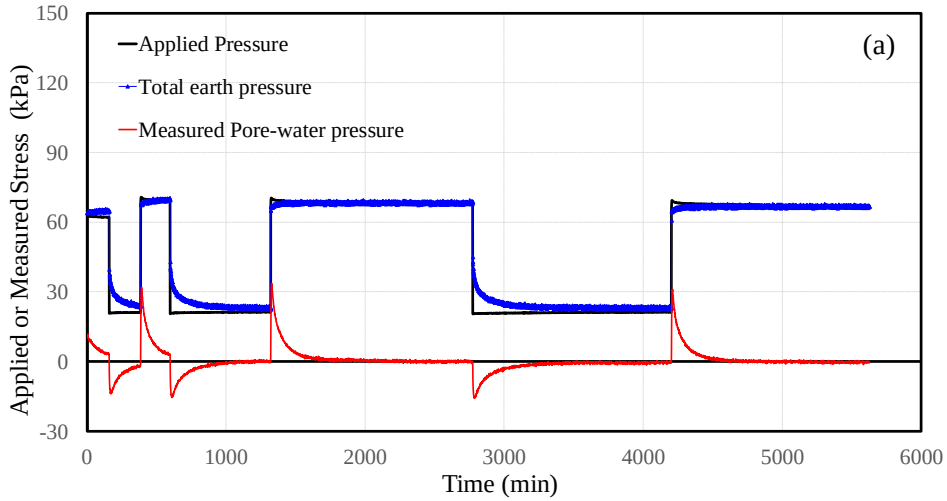

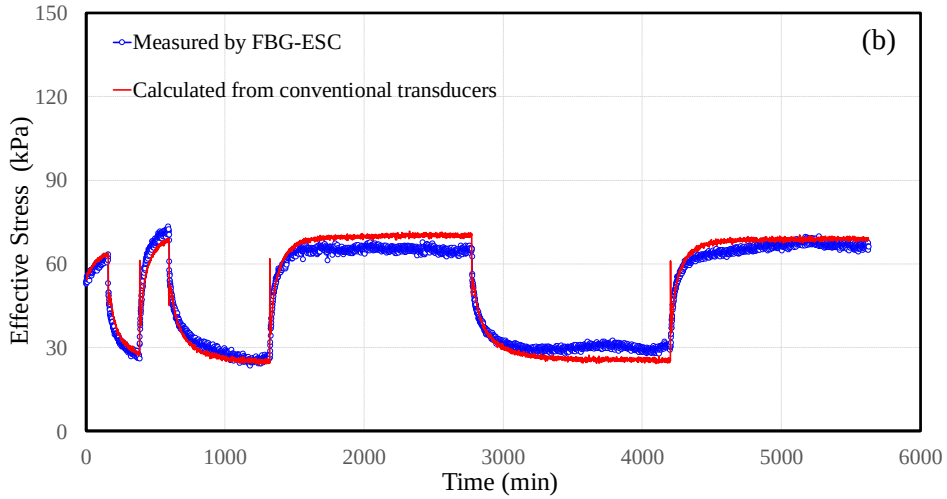

Figure 10. Test results under the complex loading conditions: (a) the applied pressure, measured total earth pressure and pore-water pressure and (b) comparison of the calculated effective stress based on the data of conventional transducers and the measured effective stress from FBG-ESC

Figure 11. Test results under the complex loading conditions: (a) the applied pressure, measured total earth pressure and pore-water pressure and (b) comparison of the calculated effective stress based on the data of conventional transducers and the measured effective stress from FBG-ESC

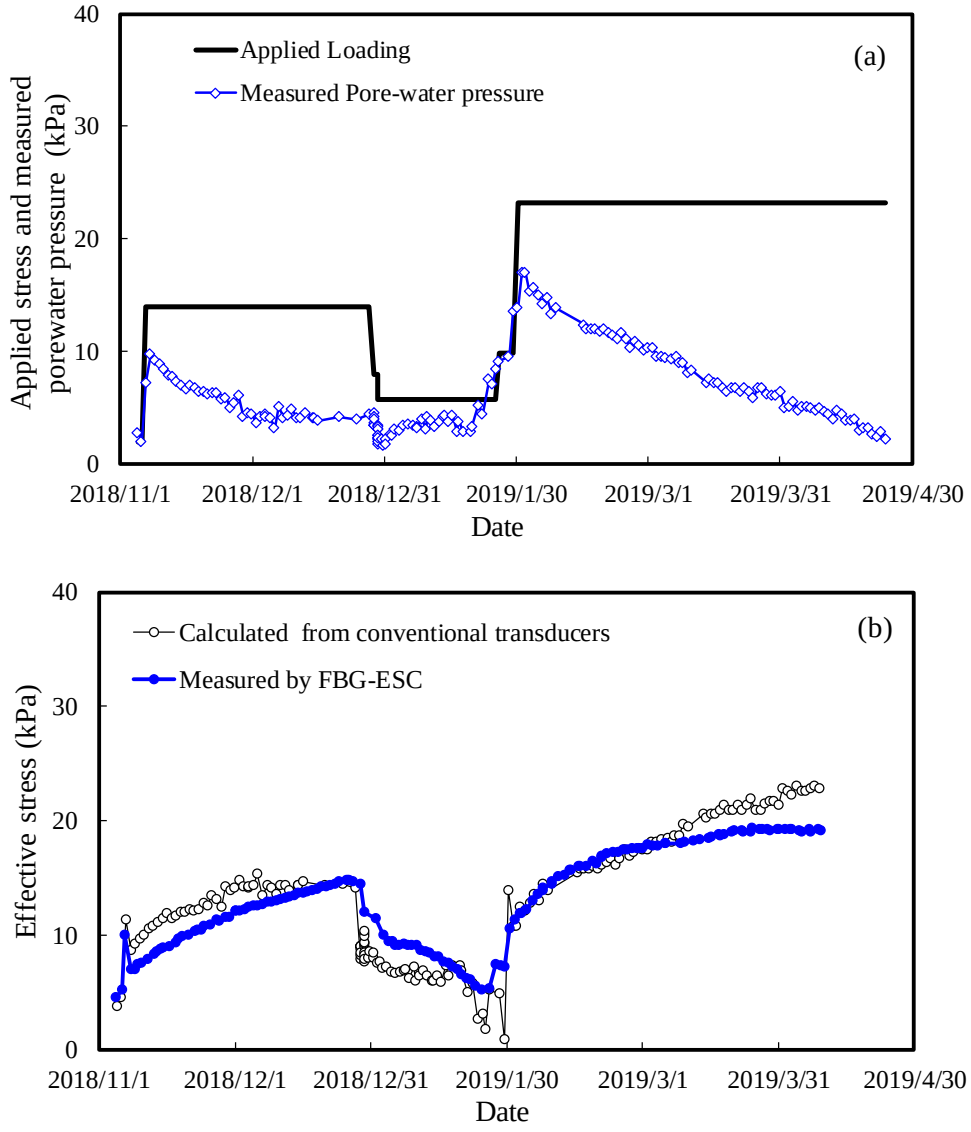

Figure 12. Test results under the complex loading conditions in the physical model under plane strain condition: (a) the applied or measured pressure *versus* time and (b) comparison of the calculated effective stress and the measured effective stress from FBG-ESC *versus* time

438

439 Table 1 Properties of the CDG soil used in the physical model test

Specific gravity	Plastic limit (%)	Liquid limit (%)	Particle Size Distribution			
			Gravel (%)	Sand (%)	Silt (%)	Clay (%)
2.65	23.4	33.1	6.9	45.2	30.5	17.4

440

441

442

443

444

445

446